Thermal and induced flow characteristics of radio frequency surface dielectric barrier discharge plasma actuation at atmospheric pressure*

Wei-long Wang(王蔚龙), Jun Li(李军), Hui-min Song(宋慧敏)†,
Di Jin(金迪), Min Jia(贾敏), and Yun Wu(吴云)

Science and Technology on Plasma Dynamics Laboratory, Air Force Engineering University, Xi'an 710038, *China*

(Received 9 July 2016; revised manuscript received 21 September 2016; published online 30 November 2016)

Thermal and induced flow velocity characteristics of radio frequency (RF) surface dielectric barrier discharge (SDBD) plasma actuation are experimentally investigated in this paper. The spatial and temporal distributions of the dielectric surface temperature are measured with the infrared thermography at atmospheric pressure. In the spanwise direction, the highest dielectric surface temperature is acquired at the center of the high voltage electrode, while it reduces gradually along the chordwise direction. The maximum temperature of the dielectric surface raises rapidly once discharge begins. After several seconds (typically 100 s), the temperature reaches equilibrium among the actuator's surface, plasma, and surrounding air. The maximum dielectric surface temperature is higher than that powered by an AC power supply in dozens of kHz. Influences of the duty cycle and the input frequency on the thermal characteristics are analyzed. When the duty cycle increases, the maximum dielectric surface temperature increases linearly. However, the maximum dielectric surface temperature increases nonlinearly when the input frequency varies from 0.47 MHz to 1.61 MHz. The induced flow velocity of the RF SDBD actuator is 0.25 m/s.

Keywords: radio frequency discharge, temperature distribution, induced flow velocity, plasma aerodynamic actuation

PACS: 52.50.Qt, 52.80.Mg, 47.80.Jk **DOI:** 10.1088/1674-1056/26/1/015205

1. Introduction

Over the past two decades, plasma flow control based on plasma aerodynamic actuation has become one of the hotspots on the performance improvement of aircraft.[1–3] The radio frequency (RF) surface dielectric barrier discharge (SDBD) has several advantages such as stable volume discharge in high-speed airflow, high energy coupling efficiency to the ionized gas, and so on. Leonov *et al*. revealed the specific regime of filamentary RF discharge plasma in supersonic airflow, the temperature of the filamentary RF plasma was found to reach as high as 4000 K at 120 Torr.[4,5]

At present, there is some research published on the temperature of plasma discharge through different measurements.[6–10] Borghi *et al*. found that the gas temperature obtained by thermography and the rotational temperature obtained by spectroscopy were approximately equal. The shape and size of the dielectric surface showed negligible effects on the gas temperature obtained by thermography.[6] Joussot *et al.* measured the surface temperature in the airflow, and the results showed that heat dissipation was less in the laminar boundary layer than in the turbulent boundary layer.[7] Dong *et al.* performed dielectric surface temperature measurements by a thermocouple, and the temperature increased about 70 °C in the experiment.[8] Tirumala *et al.* reported that heat transfer downstream the dielectric surface was dominated by convection. The surface temperature was higher when the actuator was powered by a square wave, suggesting that the heat generation was closely related to the ionization in the glow discharge regime.[9]

DBD actuated by an AC power supply in dozens of kHz can produce an induced flow along the surface of the dielectric, which is expected to control the boundary layer transition.[11,12] Debien *et al*. measured the induced flow velocity, which was as high as 10.5 m/s powered by a 1.5 kHz sinusoidal waveform.[13] Dedrick *et al.* found that the velocity of the induced flow was maximized when the RF pulses (13.56 MHz) were positioned at the peaks of the low frequency waveform, but the maximized velocity was only about 0.42 m/s.[14] So far, the studies are mostly conducted by using a power supply in dozens of kHz, the thermal and induced flow characteristics of the RF SDBD are still insufficiently investigated.

In this paper, the thermal and induced flow characteristics of the RF discharge are investigated to extend the fundamental understanding on the thermal aspects of the RF SDBD actuator. At atmospheric pressure, the relationship between the dielectric surface temperature and the discharge parameters, like duty cycle and input frequency, is discussed. Besides, the induced flow velocity of the RF SDBD actuator is also measured.

*Project supported by the National Natural Science Foundation of China (Grant Nos. 11472306, 51407197, and 51507187).
†Corresponding author. E-mail: min_cargi@sina.com
© 2017 Chinese Physical Society and IOP Publishing Ltd

2. Experimental setup

The schematic diagrams of the experimental setup and the plasma actuator are shown in Fig. 1. The plasma actuator is supplied by an RF generator/amplifier (AG 1017L, T&C), its output power increases nonlinearly from 0 to 200 W, and the operating frequency varies from 10 kHz to 10 MHz. The experiments are operated in the burst mode, in which the burst period (T_M) changes from 1 ms to 50 ms, and the burst width (T_A) ranges between 1 μs and 500 μs. T_A/T_M is defined as the duty cycle of the RF generator. To realize the impedance matching between the RF generator and the plasma actuator, a transformer matching circuit is designed.

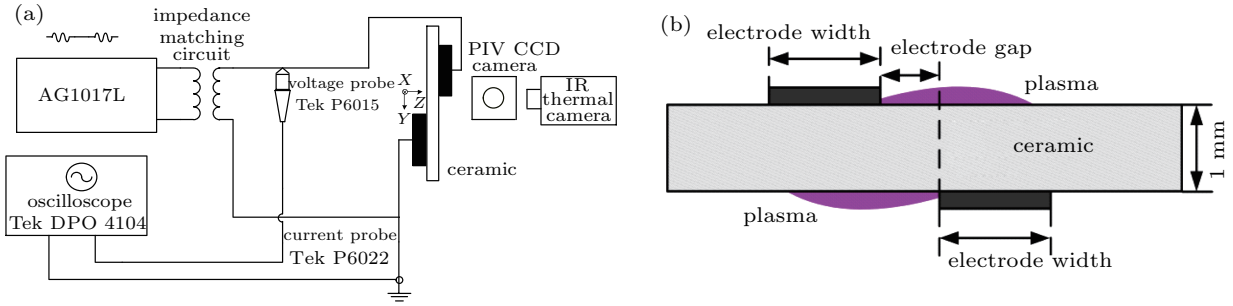


Fig. 1. (color online) Schematic diagrams of (a) the experimental setup and (b) the plasma actuator.

The applied voltage and the discharge current are measured with a high-voltage probe (Tektronix, P6015A) and a current probe (Tektronix, Tek P6022), respectively. All the signals are displayed and recorded by a digital oscilloscope (Tektronix, DPO4104). The dielectric surface temperature is obtained with a FLIR SC7300M infrared thermal imager, whose spectral range is from 3.7 μm to 4.8 μm. The infrared thermal imager is equipped with an MCT IR photo-detector composed of a 320×256-pixel array, and the temperature between −10 °C and 1500 °C can be measured. During the experiment, it is placed 50 cm away from the actuator parallel to the z axis. The induced flow velocity of the RF discharge is measured by particle image velocimetry (PIV), which employs a double pulse Nd: YAG laser. A CCD camera (1024×1280 pixels) is used to detect the laser light scattered from smoke cake solid particles. The velocity fields are obtained by the average calculation of 80 PIV image pairs.

The plasma actuator consists of a dielectric barrier and two identical electrodes as shown in Fig. 1(b). The dielectric barrier is made of a 1-mm-thick ceramic plate with a relative permittivity of 9.5. The tungsten electrode is 27 mm in length and 2 mm in width. The electrodes are separated by a ceramic dielectric barrier with an electrode gap of 1 mm.

3. Results and discussion

The experiment is performed under atmospheric pressure at ambient temperature 22 °C.

3.1. Spatial and temporal distributions of dielectric surface temperature

In this research, the dielectric plate is quite near the infrared thermal imager, so the atmospheric absorption caused by the steam and CO_2 is negligible, and the transmission coefficient of the atmosphere can be taken as 1.[15] The relationship between the temperature measured by the infrared thermal imager (T_c) and the actual temperature of the dielectric (dielectric surface temperature T_d) is described as[15]

$$T_c^4 = \varepsilon T_d^4 + (1-\varepsilon)T_e^4, \tag{1}$$

where T_e is the environmental temperature, and ε is the emissivity of the dielectric. Since the dielectric is made of ceramic with emissivity about 0.95, the temperature detected by the infrared thermal imager is approximately equal to the dielectric surface temperature. Due to the high emissivity, the measurements of the infrared thermal imager are hardly disturbed by ambient reflections.

3.1.1. Spatial distribution of dielectric surface temperature

Figure 2 shows the spatial distribution of the dielectric surface temperature when the duty cycle is 1:15 and the operating time is 100 s. In Fig. 2(a), the black rectangle represents the high-voltage electrode, the red area shows the shape of the discharge region, which covers the edge of the high-voltage electrode and spreads along the Y axis. It is also observed that the maximum dielectric surface temperature is located near the edge of the high-voltage electrode where RF discharge occurs. In Fig. 2(c), the dielectric surface temperature reduces gradually along the chordwise (Y) direction, which is also observed by Rakshit Tirumala.[9] The dielectric surface temperature plots along the spanwise (X) direction at five different Y positions are shown in Fig. 2(b). Along the spanwise direction, the dielectric surface temperature first increases and then decreases. The dielectric surface temperature is maximum at about $X = 18$ mm, which means that the RF discharge strength is strongest in the central area of the electrode. The above results are different from the spanwise temperature plots

actuated by an AC power supply at 1 kHz, and the surface temperature fluctuations are small in the discharge area.[7]

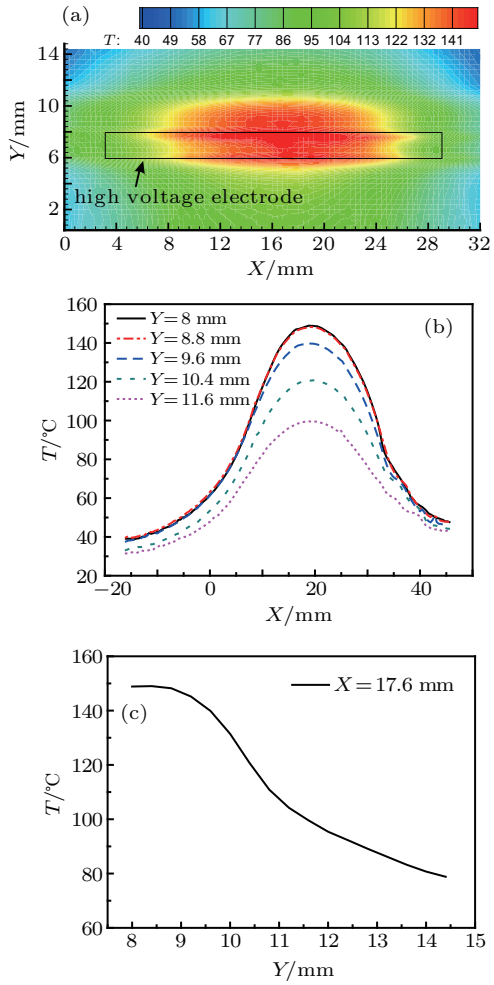


Fig. 2. (color online) The spatial dielectric surface temperature distribution of RF SDBD. Other parameters are frequency 1.70 MHz, load power 131 W, and operating time 100 s. (a) Thermal image with duty cycle of 1:15. (b) Dielectric surface temperature along the spanwise (X) direction at five different Y positions. (c) Dielectric surface temperature along the chordwise (Y) direction at $X = 17.6$ mm.

3.1.2. Temporal distribution of dielectric surface temperature

Figure 3 shows the temporal variation of the maximum dielectric surface temperature. The four curves correspond to the maximum dielectric surface temperature under different operating frequencies. At first the dielectric surface temperature rapidly increases, and some spikes are observed on the dielectric surface temperature curves. Then the raising rate of the dielectric surface temperature becomes lower, and the temperature basically reaches equilibrium at 100 s among the actuator's surface, plasma, and ambient air, which is in accordance with the result of Borghi *et al.*[6] After discharge starting, the temperature distribution is not uniform near the electrodes, and irregular filamentary discharge leads to temperature fluctuation. When the temperature reaches equilibrium, the plasma temperature equals to the dielectric surface temperature, and the spikes in the temperature curves disappear.

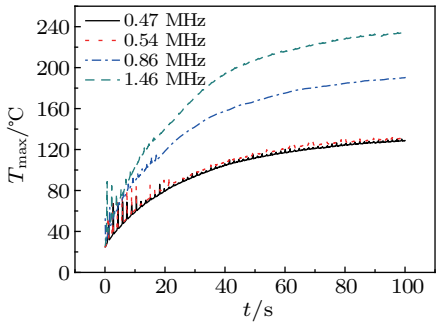


Fig. 3. (color online) Maximum dielectric surface temperature versus time for four frequencies.

3.2. Influence of duty cycle on thermal characteristics

The voltage–current waveform of RF discharge is presented in Fig. 4, where T is the single period of the voltage waveform. The variation of the duty cycle only changes the duration of the blank output ($T_A - T_M$), while T_A and T remain unchanged. The Lissajous figure is determined by the voltage–current waveform, and the effective capacitance and energy per cycle are calculated by the Lissajous figure. Since the single voltage–current waveforms are fixed under different duty cycles, the duty cycle (T_A/T_M) of the RF generator has little effect on the electrical characteristics.[16,17]

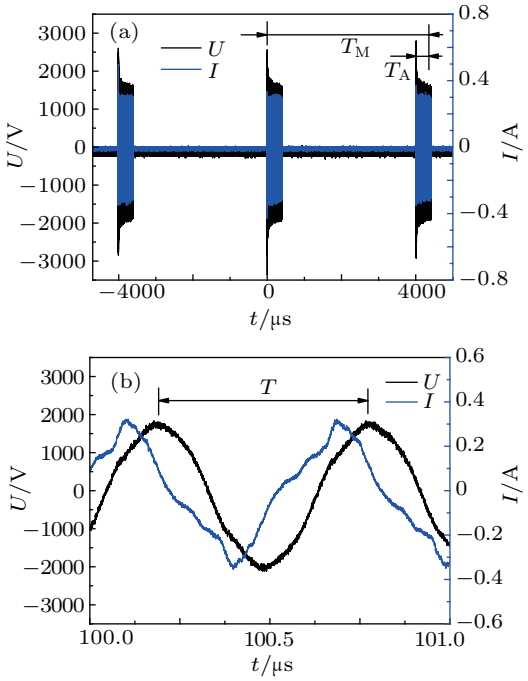


Fig. 4. (color online) (a) Voltage–current waveforms of RF SDBD with duty cycle 1:10. (b) The voltage–current waveforms in the single period.

Figure 5 presents the spatial evolution of the dielectric surface temperature after 100 s discharge at different duty cycles. The frequency of the RF generator is 1.70 MHz and the load power is 131 W. The maximum dielectric surface temperature (227 °C in Fig. 5(a)) is located near the edge of the high-voltage electrode, which is higher than that generated with the AC power supply of 1 kHz.[7] With the increase of the duty cycle, the dielectric surface temperature rises obviously.

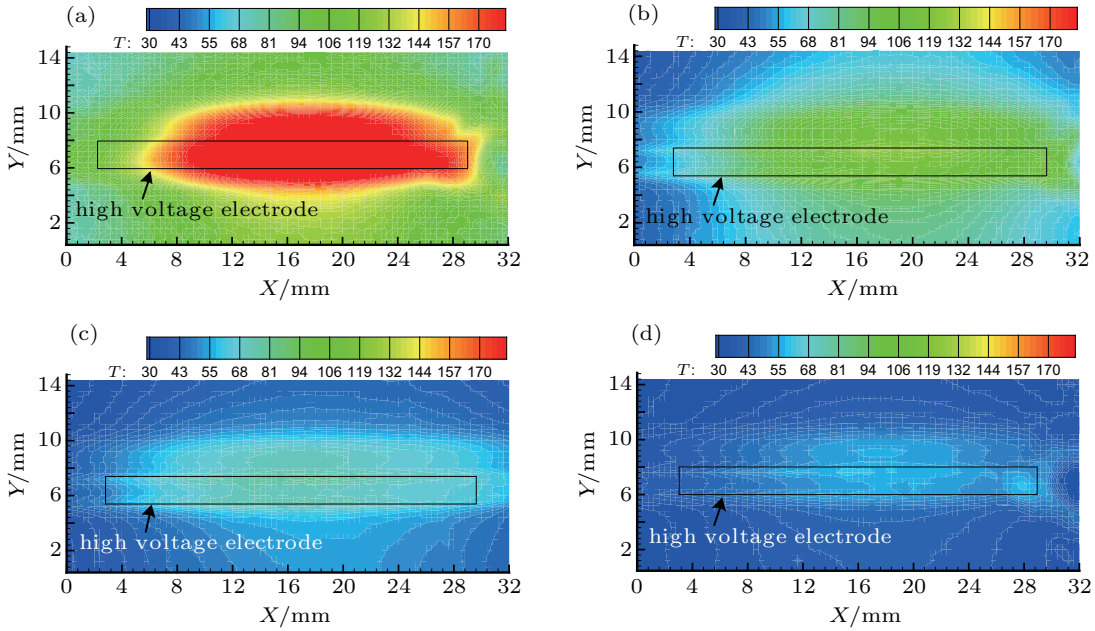


Fig. 5. (color online) RF discharge thermal images of the absolute dielectric surface temperature at different duty cycles: (a) 1:10, (b) 1:20, (c) 1:30, (d) 1:40.

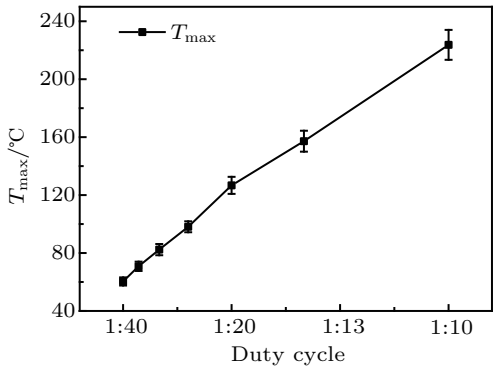


Fig. 6. The maximum dielectric surface temperatures at different duty cycles.

As shown in Fig. 6, a linear relationship is observed between the temperature and the duty cycle. When the duty cycle increases, the burst width (T_A) remains unchanged, while the duration of the blank output (T_A–T_M) is shorter as shown in Fig. 4. The heating time of plasma discharge is longer at the higher duty cycle, so the dielectric surface temperature increases with the increase of the duty cycle.

3.3. Influence of frequency on thermal characteristics

The influence of the frequency on the RF SDBD is studied. At the duty cycle 1:10 and load power 131 W in quiescent air, the thermal images and voltage–current waveforms of RF

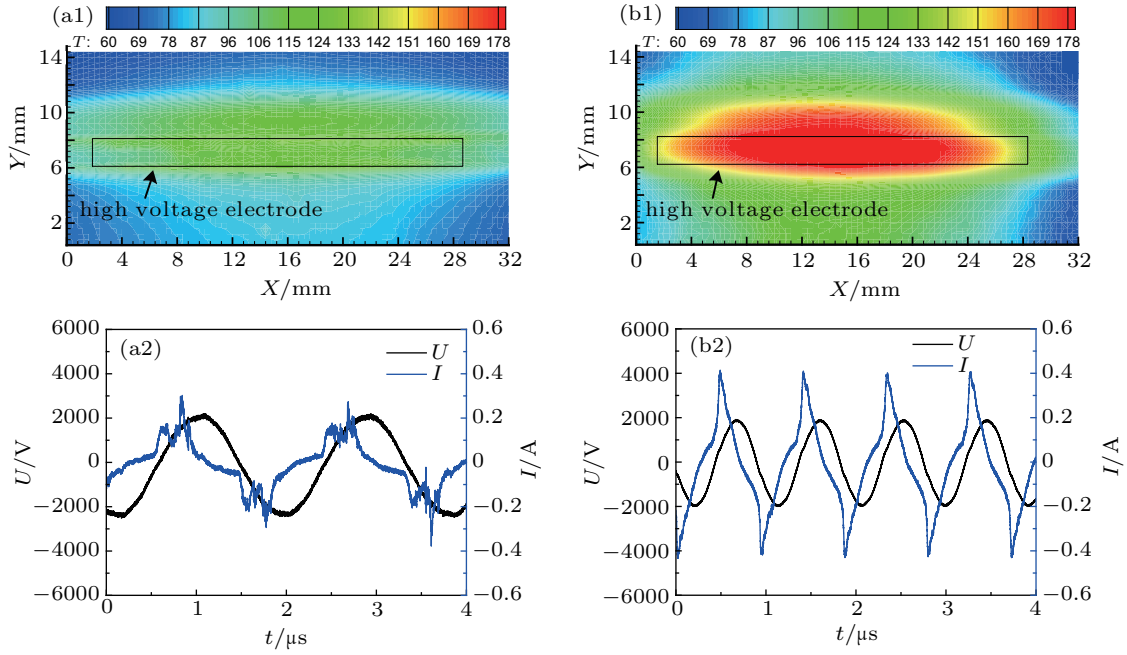


Fig. 7. (color online) Thermal images and voltage–current waveforms of RF discharge at different frequencies: (a) 0.54 MHz, (b) 1.13 MHz.

discharge are shown in Fig. 7, the discharge frequencies are 0.54 MHz and 1.13 MHz, respectively. The maximum dielectric surface temperature is about 132 °C with the frequency of 0.54 MHz. When the frequency rises to 1.13 MHz, the maximum dielectric surface temperature reaches 201 °C. It is concluded that the surface temperature ascends with the increase of the frequency. When the frequency is 1.13 MHz, the current has only one peak. As the frequency decreases to 0.54 MHz, there are many irregular spikes in the current curve, and the peak–peak current value decreases. The current is higher at higher frequency, and the heating power increases with the increase of the current. As the frequency ascends, the heating power and the surface temperature ascend. At different frequencies, the voltage waveforms are all smooth sine waves without distinct changes.

The heat generated in plasma depends on the frequency when the voltage is fixed. Figure 8 shows that a higher frequency can result in a higher dielectric surface temperature, but a non-linear relationship is observed between the dielectric surface temperature and the frequency for these cases. However Tirumala *et al.* observed a linear relationship with the frequency varying between 200 Hz and 1600 Hz.[7]

When the frequency varies, the impedance matching characteristics between the RF generator and the actuator also change. Although the load power remains unchanged, the power fed back to the RF generator still varies, which leads to the change of the actual power loading on the actuator. So with the increase of the frequency, the maximum dielectric surface temperature increases nonlinearly.

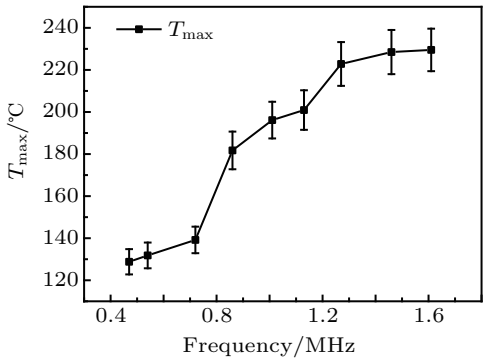


Fig. 8. The maximum dielectric surface temperatures at different frequencies.

3.4. Induced flow characteristics at atmospheric pressure

The spatial variation of the time-averaged induced flow velocity near the actuator is shown in Fig. 9(a). The frequency of the RF generator is 1.70 MHz and the load power is 131 W at atmospheric pressure. The high-voltage electrode is marked by the black rectangle and it is located at about $Y = 17$ mm. The maximum value of v_y is 0.25 m/s, which is in accordance with the velocity actuated by a 13.56 MHz RF pulse generator,[14] but much smaller than the velocity actuated by the AC power supply of dozens of kHz.[18] Figure 9(b) shows that v_y rises linearly with the increase of the duty cycle. Both dielectric surface temperature and induced flow velocity increase at higher duty cycle.

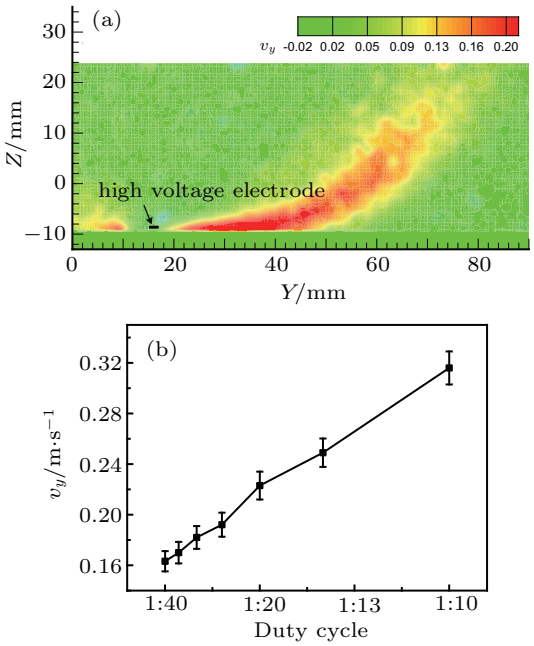


Fig. 9. (color online) The component of the induced flow velocity in the y direction (v_y) with RF SDBD. (a) Time-averaged induced flow velocity field above the RF SDBD actuator with duty cycle of 1:15. (b) Time-averaged induced flow velocity at different duty cycles.

It should be noted that compared with SDBD in dozens of kHz, the induced flow velocity powered by the RF generator is pretty small, indicating that the mechanism in the RF plasma flow control may not be the near-wall plasma induced flow. However the RF plasma temperature is higher than that of the other generator as discussed above. It is quite possible that the surface heating of the RF plasma may influence the supersonic flow structure and improve the performance of supersonic aircrafts.[15,19,20]

4. Conclusions

The thermal and the induced flow characteristics of RF SDBD plasma at atmospheric pressure are experimentally investigated. The main conclusions are as follows.

Under different duty cycles and frequencies, the dielectric surface temperature is highest at the center of the electrode, and decreases towards both of its sides. Along the chordwise (Y) direction, the dielectric surface temperature gradually decreases. In quiescent air, at first the dielectric surface temperature shows a significant increase after RF discharge. Then the temperature raising rate gradually becomes smaller. About 100 s later, the temperature reaches equilibrium among the actuator's surface, plasma, and surrounding air.

As the duty cycle increases, the dielectric surface temperature ascends linearly. The maximum surface temperature

(227 °C) of RF SDBD is higher than that powered by the AC power supply in dozens of kHz. When the frequency is high, the current waveforms have only one peak. As the frequency decreases to 0.54 MHz, many irregular spikes are observed. The dielectric surface temperature increases nonlinearly with the increase of the frequency.

The induced flow velocity of RF SDBD in the Y-direction ascends linearly with the increase of the duty cycle, but the maximum induced flow velocity (0.25 m/s) is much lower than that powered by the AC power supply in dozens of kHz. The induced flow velocity of RF discharge has little influence on the plasma flow control, however, the heating effect of the RF discharge plasma shows significant potential on the supersonic flow control.

Future work should focus on the characteristics of RF discharge plasma actuation in supersonic flow, and the interaction mechanism between RF discharge plasma and supersonic shockwave in order to enhance its flow control ability.

References

[1] Roth J R 2003 *Phys. Plasmas* **10** 2117
[2] Patel M P, Ng T T and Vasudevan S 2007 *J. Aircraft* **44** 1264
[3] Li Y H, Wu Y, Zhu J Q, Zhou M, Su C B, Zhang X W and Zhu J Q 2010 *Exp. Fluids* **48** 1015
[4] Leonov S, Bityurin V, Klimov A, Kolesnichenko Y and Yuriev A 2001 *32th AIAA Plasmadynamics and Lasers Conference*, June 11–14, 2001, Anaheim, SUA, p. 057
[5] Leonov S and Yarantsev D A 2008 *J. Propul. Power* **24** 1168
[6] Carlo A B, Andrea C, Chiara L, Gabriele N, Alessandro G and Roberto P 2010 *41st Plasmadynamics and Lasers Conference*, June 28-July 1, 2010, Chicago, USA, p. 4763
[7] Joussot R, Hong D, Rabat H, Boucinha V, Weber R R and Leroy C A 2010 *40th Fluid Dynamics Conference and Exhibit*, June 28-July 1, 2010, Chicago, USA, p. 5102
[8] Dong B, Bauchire J M, Pouvesle J M, Magnier P and Hong D 2008 *J. Phys. D: Appl. Phys.* **41** 155201
[9] Rakshit T, Nicolas B, Eric M, Matthieu F, Gildas L and Eva D 2014 *J. Phys. D: Appl. Phys.* **47** 255203
[10] Scott A S, James M, Charles D J, Roger L K and James R H 2009 *AIAA J.* **47** 1107
[11] Duchmann A, Grundmann S and Tropea C 2013 *Exp. Fluids* **54** 1461
[12] Wang J, LI Y H, Chen B Q, Su C B, Song H M and Wu Y 2009 *39th AIAA Fluid Dynamics Conference and Exhibite*, June 22-25, 2009, San Antonio, USA, p. 4286
[13] Debien A, Benard N and Moreau E 2012 *J. Phys. D: Appl. Phys.* **45** 215201
[14] Dedrick J, Im S, Cappelli M, Boswell R W and Charles C 2013 *IEEE Trans. Plasma Sci.* **41** 3275
[15] Joussot R, Lago V and Parisse J D 2015 *Exp. Fluids* **56** 102
[16] Kriegseis J, Möller B, Grundmann S and Tropea C 2011 *J. Electrostat.* **69** 302
[17] Wang W L, Song H M, Li J, Jia M, Wu Y and Jin D 2016 *Chin. Phys. B* **25** 045203
[18] Forte M, Jolibois J, Pons J, Moreau E, Touchard G and Cazalens M 2007 *Exp. Fluids* **43** 917
[19] Menier E, Leger L, Depussay E, Lago V and Artana G 2007 *J. Phys D: Appl. Phys.* **40** 695
[20] Leger L and Depussay E 2012 *Exp. Fluids* **53** 699
[21] Dedrick J, Boswell R W, Audier P, Rabat H, Hong D and Charles C 2011 *J. Phys. D: Appl. Phys.* **44** 205202